Surface Science 648 (2016) 236–241

Contents lists available at ScienceDirect

Surface Science

journal homepage: www.elsevier.com/locate/susc

Kinetics of low-temperature CO oxidation on Au(111)

Theodore Thuening [a], Joshua Walker [a], Heather Adams [a], Octavio Furlong [b], Wilfred T. Tysoe [a,*]

[a] Department of Chemistry and Biochemistry and Laboratory for Surface Studies, University of Wisconsin-Milwaukee, Milwaukee, WI 53211, USA
[b] Department of Physics, Laboratorio de Ciencias de Superficies y Medios Porosos, Universidad Nacional de San Luis, Chacabuco 917, 5700 San Luis, Argentina

ARTICLE INFO

Article history:
Received 24 July 2015
Received in revised form 25 November 2015
Accepted 13 December 2015
Available online 22 December 2015

Keywords:
Au(111)
Oxygen
Carbon monoxide
Temperature-programmed desorption
Reflection-absorption infrared spectroscopy

ABSTRACT

The oxidation of carbon monoxide on oxygen-modified Au(111) surfaces is studied using a combination of reflection-absorption infrared spectroscopy (RAIRS) and temperature-programmed desorption (TPD). TPD reveals that CO desorbs in two states with the low-temperature state have a peak temperature between ~130 and 150 K, and the higher-temperature state having a peak temperature that varies from ~175 to ~220 K depending on the initial oxygen and CO coverages. Infrared spectroscopy indicates that the low-temperature CO desorption state is predominantly associated with CO adsorbed on $Au^{\delta+}$ sites, while the higher-temperature states are due to CO on Au^0 sites. No additional vibrational features are detected indicating that CO reacts directly with adsorbed atomic oxygen on gold to form CO_2. Estimates of the activation energy for CO_2 formation suggest that they are in the same range and found for supported gold catalysts at reaction temperature below ~300 K.

1. Introduction

The Somorjai group pioneered the idea that the flexibility and restructuring of metal surfaces was crucial to its catalytic activity and proposed the notion that adsorption on the surface caused structural changes in the metal surface that caused it to become more active [1–6]. In particular, gold surfaces have been found to undergo very significant adsorbate-induced structural changes [7–10]. Consequently, while bulk gold is a noble metal and is considered to be unreactive, oxide-supported gold nanoparticles have been found to have quite remarkable catalytic activity for a number of reactions [11–14]. In particular, it forms the basis for active CO oxidation catalysts [11,15–24]. Water has been suggested to play a role in accelerating the rate of CO oxidation [24–27] and has been studied primarily using molecular beam methods on Au(111) [28,29]. Previous work has also been carried out to explore carbon monoxide oxidation on gold surfaces in the absence of water [30,31].

It has been suggested that oxygen is activated by dissociating either directly on low-coordination sites on the gold [32–34] or on the oxide support and spilling over to the metal to then oxidize CO [34,35]. In addition, it has been proposed that CO_2 can form *via* an intermediate $Au_2CO_3^-$ carbonate complex rather than by a simple addition of adsorbed atomic oxygen to adsorbed carbon monoxide [36–38].

Since carbon monoxide adsorbs very weakly on low Miller index gold surfaces [39–42], but more strongly on step sites [39], reaction on Au(111) might not be expected to occur in temperature-programmed desorption (TPD) so that experiments have been performed primarily using molecular beams of carbon monoxide incident on a gold-covered surface [28,29,31]. However, as shown below, the adsorption of carbon monoxide on Au(111), in particular in the presence of co-adsorbed oxygen, is sufficiently strong that both TPD and reflection-absorption infrared spectroscopy (RAIRS) can be used to explore the reaction pathway.

Controlled atomic oxygen coverages are obtained by exposing the surface to ozone [43], containing molecular oxygen, which does not adsorb at room temperature. TPD experiments show the direct oxidation of carbon monoxide on the gold surface, thereby allowing desorption and reaction activation energies to be estimated [44]. This also enables the surface to be interrogated using RAIRS over the same temperature range as that at which the oxidation chemistry occurs to search for any reaction intermediates such as carbonates since their vibrational frequencies [45] are distinct from those for CO on gold [46].

2. Experimental methods

The apparatus used to collect RAIRS and TPD data has been described in detail elsewhere [47]. Infrared spectra were collected using a Bruker Equinox spectrometer, typically for 1000 scans at a resolution of 4 cm^{-1}. TPD data were collected using a Dichor quadrupole mass spectrometer interfaced to a computer that allowed up to five masses to be monitored sequentially in a single experiment. The sample could be cooled to 80 K by thermal contact to a liquid nitrogen-filled reservoir and resistively heated to ~1200 K.

A Au(111) single crystal (Princeton Scientific) was cleaned with cycles of ion bombardment using 1 keV argon ions for 30 min (1 μA/cm^2), annealing to 900 K for 5 min and then to 600 K for 30 min. Ozone was produced by an A2Z Ozone Inc., 5GLAB ozone generator where the

* Corresponding author. Tel.: +1 414 229 5222; fax: +1 414 229 5036.
E-mail address: wtt@uwm.edu (W.T. Tysoe).

http://dx.doi.org/10.1016/j.susc.2015.12.010
0039-6028/

output of the generator was connected *via* a Teflon tube directly to a high-precision variable leak valve through a 1-mm-diameter glass tube that was directed at the inlet of the leak valve to minimize ozone decomposition. The ozone was returned through an external concentric glass tube and led though a Teflon tube to a fume hood. The proportion of ozone in the gas mixture was maximized by monitoring the 32 (O_2^+) and 48 (O_3^+) signals in the mass spectrometer located inside the vacuum chamber and it is estimated that the ozone concentration in the gas mixture is ~4%.

3. Results and discussion

3.1. Oxygen adsorption from ozone on Au(111)

TPD data were collected for atomic oxygen adsorbed from ozone on Au(111) as a function of exposure. Oxygen (32 amu) desorbs in a sharp peak centered at ~540 K at low coverages and shifts to higher coverages with exposure so that at the highest coverage desorbs at ~560 K (data not shown). These desorption profiles and peak temperatures are in good agreement with previous measurements on Au(111) [43]. Measuring the oxygen coverage from the integrated area under the desorption peak compared with previous results allows the oxygen coverage to be calibrated as a function of exposure to the mixture of $O_2 + O_3$, and the results described below use oxygen coverages calibrated in this way.

3.2. Carbon monoxide oxidation on Au(111)

The oxidation of CO was explored using TPD on oxygen-covered Au(111) by adsorbing atomic oxygen using ozone [43]. A series of TPD spectra for a Au(111) sample initially containing 0.2 ML of atomic oxygen are shown in Fig. 1 as a function of CO exposure. CO (28 amu) is found to desorb in two distinct states from oxygen-covered Au(111) at ~132 and 174 K (Fig. 1A), that grow approximately equally as a function of CO exposure. This results in low-temperature CO_2 (44 amu) formation (Fig. 2B), initially in a single peak centered at ~168 K that grows with increasing CO exposure, followed by the growth of an additional CO_2 state at ~142 K. Clearly, the high-temperature CO_2 state must be associated with oxidation of the more stable CO that desorbs at ~174 K (Fig. 1A). The reaction of carbon monoxide with surface atomic oxygen is confirmed by the decrease in intensity of the remaining oxygen (32 amu) feature with increasing CO exposure (Fig. 2C).

The corresponding results for a higher oxygen coverage of 0.75 ML are shown in Fig. 2. Now the lower-temperature CO desorption state (28 amu), centered at ~153 K, is less intense than the higher-temperature CO desorption state that shifts in temperature from ~190 to ~222 K (Fig. 2A). Intense CO_2 desorption states (44 amu) are measured with a peak initially appearing at ~173 K, shifting to higher temperatures up to ~212 K as the CO exposure increases (Fig. 2B).

The effect of varying the oxygen coverage is shown in Fig. 3 for a CO exposure of 10 L, resulting in saturation of the surface with CO. Again, two CO (28 amu) desorption states are observed; a low-temperature

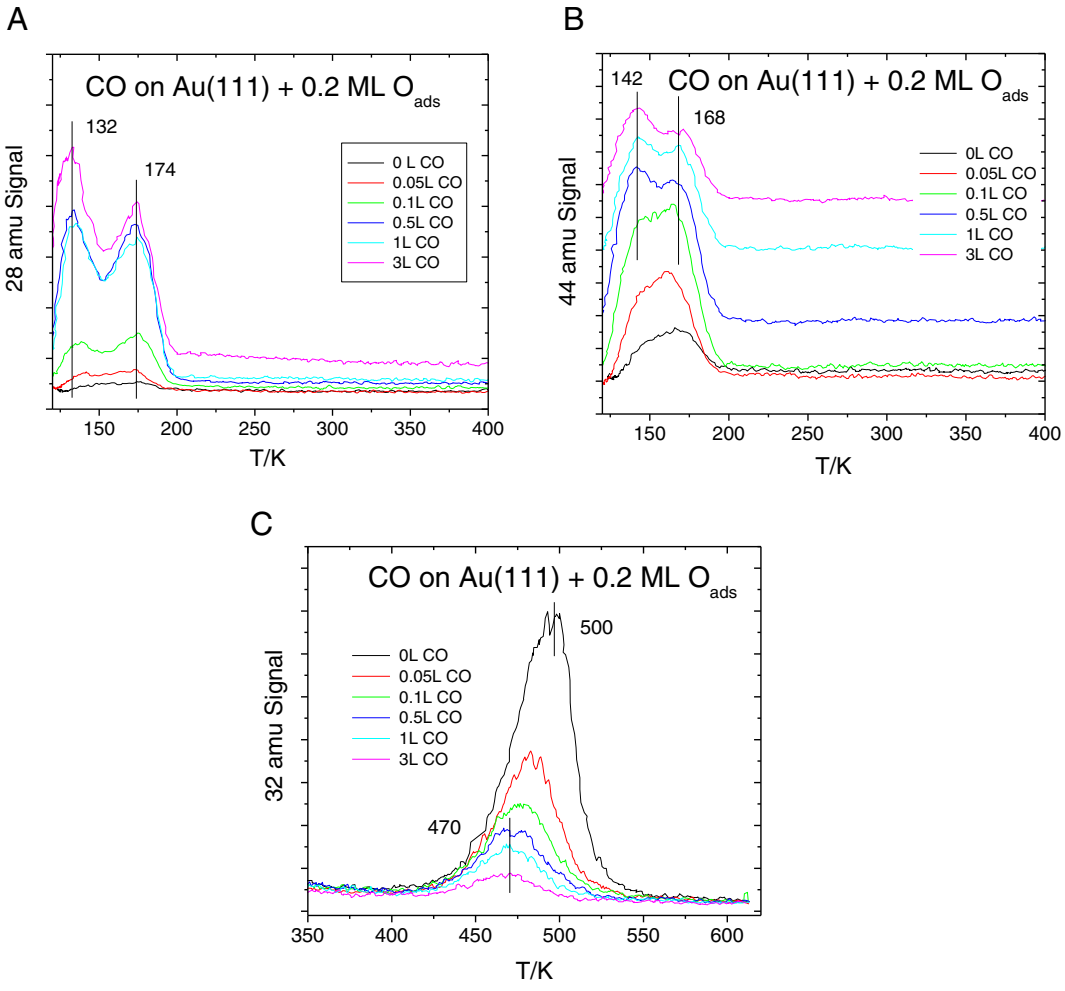

Fig. 1. TPD profiles [(A) 28 (CO), (B) 44 and (C) 32 amu] of CO adsorbed at 80 K on a surface precovered by 0.2 ML of atomic oxygen collected using a heating rate of 3.4 K/s as a function of CO exposure.

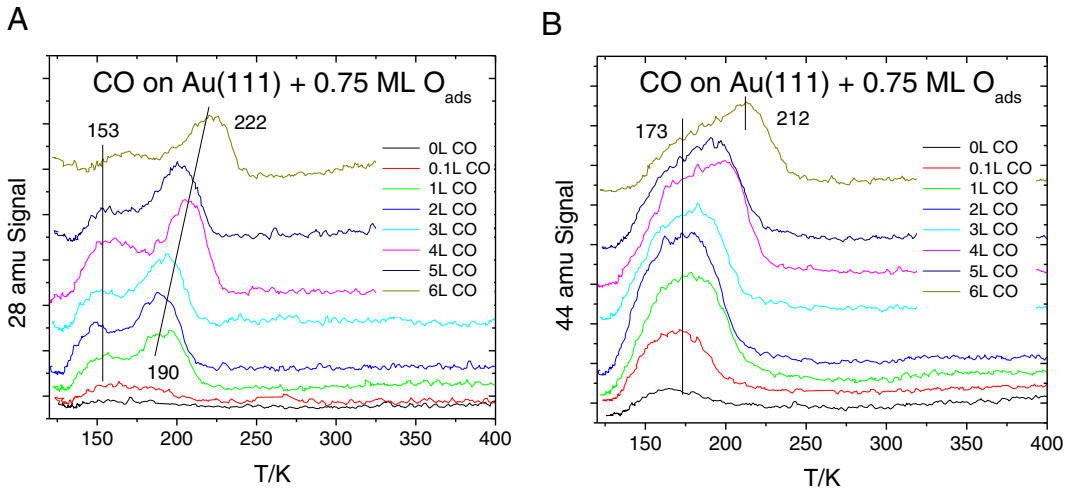

Fig. 2. TPD profiles [(A) 28 (CO) and (B) 44 amu] of CO adsorbed at 80 K on a surface precovered by 0.75 ML of atomic oxygen collected using a heating rate of 3.4 K/s as a function of CO exposure.

state centered at ~141 K that initially grows in parallel with the higher-temperature state, and then decreases in intensity for oxygen coverages above ~0.9 ML, while both states decrease in intensity at higher oxygen coverages (Fig. 3A). Carbon dioxide (44 amu) desorbs in a broad feature between ~130 and 210 K, with an intensity that grows up to an oxygen coverage of ~0.9 ML, and then decreases (Fig. 3B). The corresponding oxygen desorption profiles (32 amu) are shown in Fig. 3C, which are identical in shape to those found on clean Au(111) [43]. The resulting

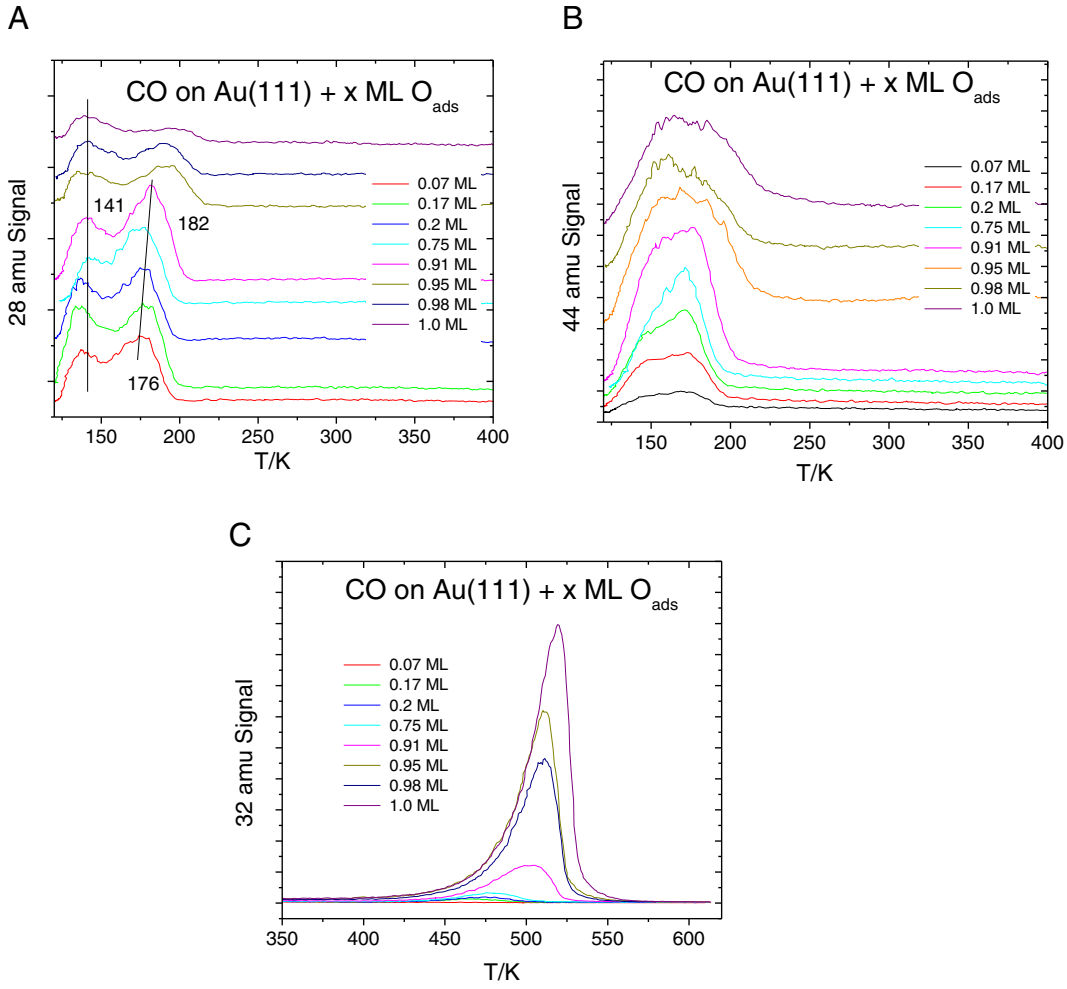

Fig. 3. TPD profiles [(A) 28 (CO), (B) 44 and (C) 32 amu] of 10 L CO adsorbed at 80 K on a surface with various coverages of atomic oxygen collected using a heating rate of 3.4 K/s as a function of CO exposure.

stoichiometric reaction between adsorbed CO and oxygen is illustrated by the data in Fig. 4. This plots the coverage of CO_2 that is produced (●) and the adsorbed oxygen that is consumed (■) as a function of oxygen coverage. Here, the coverage of oxygen consumed is measured from the area of the 32 amu profile in the presence of carbon monoxide (Fig. 3C) compared to the area for an identical oxygen dose without CO. There is good agreement between the two sets of data indicating a quantitative reaction between adsorbed oxygen and CO (Fig. 4). The carbon dioxide that is initially formed is limited by the inventory of oxygen on the surface, which is completely consumed by reaction with CO. At higher oxygen coverages, some oxygen remains on the surface so that the CO_2 yield becomes limited by the amount of carbon monoxide. However, in this case, not all of the carbon monoxide is consumed and a portion desorbs when there is still oxygen on the surface. At coverages above ~0.8 ML of oxygen, the carbon dioxide yield decreases due to the blocking of CO adsorption by atomic oxygen.

The corresponding infrared spectra for CO on clean Au(111) following adsorption at 87 K are shown in Fig. 5A. The spectrum at 87 K exhibits a peak at ~2110 cm^{-1}, close to the value of 2118 cm^{-1} found previously for low-temperature CO adsorption on Au(111) [48]. Additional spectra show the effect of heating the surface to various temperatures for 10 s and then allowing the sample to cool once again to ~87 K following which the spectrum was collected. This shows a decrease in the intensity of the infrared peaks and the inset plots the integrated absorbance of the infrared features as a function of annealing temperature. An additional shift in peak position is noted as the CO coverage changes due to a combination of dipolar coupling and chemical shifts [49,50]. The CO vibrational frequency of 2110 cm^{-1} is in good agreement with results for high pressures of CO on Au(110) [51] and for CO adsorption at low temperatures on Au(211) [39] and Au(332) surfaces [42]. However, CO adsorption on Au(111) at high pressures (up to 100 Torr) showed a single infrared mode at 2060 cm^{-1} that did not change position with coverage [41]. In this case, considerable surface restructuring was noted at those higher CO pressures [52]. It has been shown that the CO stretching frequency, while being relatively insensitive to gold coordination number, is a reasonably sensitive probe of the gold charge state [46], where Au^0-CO has a CO stretching mode between 2130 and 2090 cm^{-1} in agreement with a frequency of ~2110 cm^{-1} found in Fig. 5A.

Fig. 5B shows the CO stretching region of CO adsorbed on a surface containing 0.2 ML of oxygen as a function of CO exposure. Two infrared peaks at 2135 and 2110 cm^{-1} grow simultaneously with increasing CO exposure, corresponding to the growth of two desorption states found in TPD (Fig. 1). Comparison with the infrared spectrum on clean Au(111) (Fig. 5A) suggests that the 2135 cm^{-1} state is induced by co-adsorbed atomic oxygen while the 2110 cm^{-1} state is due to CO on unaffected sites. The appearance of the feature at ~2135 cm^{-1} is consistent with CO adsorption on $Au^{\delta+}$ sites [46], which appear at higher frequencies than CO on Au^0 sites, generally between 2150 and 2190 cm^{-1}.

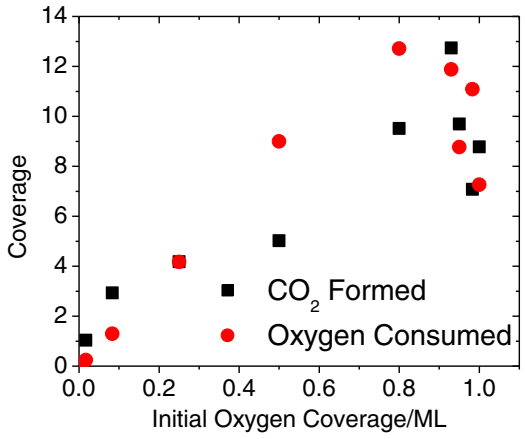

Fig. 4. Plot of the equivalent coverage of carbon dioxide produced versus the coverage of oxygen consumed due to a reaction between atomic oxygen and CO adsorbed at 80 K on oxygen-covered Au(111) as a function of oxygen coverage.

The evolution in the infrared spectra as a function of annealing temperature is shown in Fig. 5C for a saturation CO exposure of ~10 L. The results were obtained by heating to the indicated temperature and then allowing the sample to cool once again, following which the infrared spectra were collected. The higher CO coverages in this case result in additional spectral shifts compared to the data with lower CO coverages (Fig. 5B). In particular, the peak for CO on oxygen-modified sites shifts to ~2141 cm^{-1}. The variation in integrated peak area as a function of annealing temperature is shown plotted as an inset to Fig. 5C, where the peak desorption temperatures found for the same surface (Fig. 1A) are indicated. This reveals that that the low-temperature (~132 K) desorption feature in Fig. 1 is associated with CO bound to $Au^{\delta+}$ sites, while the higher temperature, ~174 K state is due to CO adsorbed on Au^0 sites.

No other vibrational modes were detected during this experiment, indicating that CO reacts directly with adsorbed atomic oxygen to form carbon dioxide without forming any stable surface intermediates.

4. Discussion

Addition of oxygen to the surface produced two distinct CO desorption states comprising a low-temperature state with a peak centered between ~130 and 150 K, and a higher-temperature state with a peak temperature that varies from ~175 to ~220 K depending on the initial oxygen and CO coverages. An analysis by Redhead [44] using an experimental heating rate and assuming a pre-exponential factor of 1×10^{13} s^{-1} yield CO desorption activation energies of 32 to 37 kJ/mol for the low-temperature state and from 44 to 56 kJ/mol for the high-temperature state. The infrared data suggest that the low-temperature states are associated with CO adsorbed on $Au^{\delta+}$ sites and the higher-temperature desorption features are due to adsorption on gold sites.

The CO 4σ, 1π and 5σ orbitals are located below the bottom of the gold d-band while the 2π* orbitals located are close to the Fermi level [53] corresponding to the conventional Blyholder model for CO adsorption on transition-metal surfaces [54]. However, the low density of states of gold near the Fermi level leads to only relatively weak back donation into the 2π* level, with CO acting as a weak π-acceptor, resulting in low binding energies. Thus, removing electron density from the gold by co-adsorbing atomic oxygen increases the energy difference between the Fermi energy and the CO 2π* orbitals, thereby weakening the bonding as found experimentally. A similar shift to higher frequencies (in this case to ~2146 cm^{-1}) has been seen for CO co-adsorbed with hydroxyl species on Au(111) [48] consistent with this bonding model.

However, creating low-coordination sites on a roughened surface can increase the binding strength of CO [55]. In fact, the desorption peak temperatures for the two CO desorption states found on oxygen-modified Au(111) are very similar to those found for gold nanoparticles on FeO [56] and on surfaces roughened by oxygen or argon ion bombardment [57] indicating that surface roughening has some influence on CO binding. It is interesting to note that the infrared spectrum of CO adsorbed on gold nanoparticles on FeO exhibits a single vibrational feature centered at ~2108 cm^{-1}, similar to the low-frequency feature found on the oxygen-covered surface (Fig. 5B and 5C). However, the CO stretching frequency on gold is notoriously insensitive to surface structure, as evidenced by the similarity between the vibrational frequency on Au(111) (Fig. 5A) and on oxygen-covered surfaces, which have been roughed by oxygen adsorption. Heating CO-covered gold nanoparticles on FeO resulted in a reduction in the intensity of the 2108 cm^{-1} peak over a temperature range that was coincident the high-temperature (~200 K) CO desorption state, while no intensity

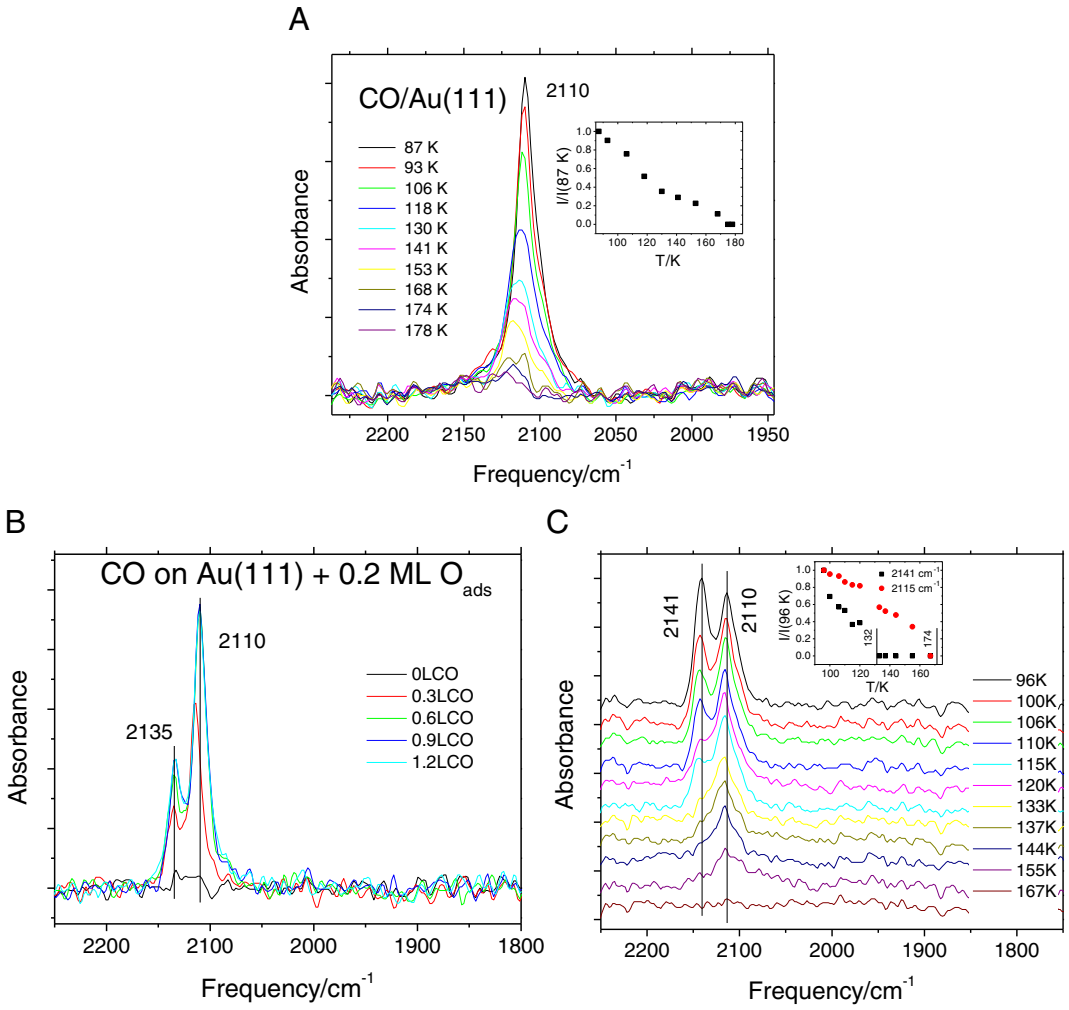

Fig. 5. (A) RAIRS spectra of CO on Au(111) at 87 K and heated to various temperatures. Inset shows the variation in integrated absorbance with temperature. (B) CO adsorbed on Au(111) with 0.2 ML of atomic oxygen as a function of oxygen exposure. (C) RAIRS spectra of a saturated overlayer of CO (~10 L exposure) on Au(111) with 0.2 ML of atomic oxygen as a function of annealing temperature. Inset shows the variation in integrated absorbances of the 2141 and 2110 cm^{-1} peaks as a function of annealing temperature.

decrease was noted when CO desorbed at lower temperatures. This was ascribed to the weakly bound CO that desorbs at ~130 K, but which lies parallel to the surface, and is thus infrared forbidden [56,58].

In the case of oxygen-modified Au(111), the ~2141 cm^{-1} vibrational mode, assigned to CO adsorption on $Au^{\delta+}$ sites, decreases in intensity coincident with the low-temperature CO desorption peak but does not exclude the possibility of there also being some infrared-invisible CO also being present on the surface.

Adsorbed CO reacts quantitatively with adsorbed atomic oxygen to form carbon dioxide (Fig. 4) where the amount of carbon dioxide initially increases with oxygen coverage but decreases at higher coverages due to site blocking similar to the behavior found previously for CO oxidation on Au(111) using molecular beams of CO [31]. No intermediate surface species are detected following CO adsorption on oxygen-covered Au(111), indicating that CO_2 is formed by a direct coupling between CO and adsorbed oxygen to immediately desorb CO_2 [59]. The carbon dioxide that is formed desorbs over the same range as CO suggesting that the activation energies for CO_2 formation also lie approximately in the range of ~32 to 56 kJ/mol and is in the same range as the activation energies for CO oxidation on gold nanoparticle catalysts for reaction carried out below ~300 K [23]. In particular, the CO_2 formation temperatures in TPD are much lower than those found on main group transition metals where it forms between 300 and 500 K on Rh(111) [60], between 400 and 500 K on Ni(111) [61], from 200 to 500 K on Pd(111) [62] and at ~350 K on Pt(111) [63].

5. Conclusions

Combined infrared and TPD experiments reveal that Au(111) single crystals exposed to ozone to form adsorbed atomic oxygen can oxidize CO to CO_2 at temperatures as low as ~140 K. CO desorbs in two states where the low-temperature state is assigned to CO adsorbed on $Au^{\delta+}$ sites and the higher-temperature desorption features are due to adsorption on gold sites. This observation is consistent with the Blyholder model. However, the low-temperature state may also include contributions from infrared-invisible CO bound with its axis parallel to the surface.

Carbon dioxide forms over the same temperature range as that at which CO desorbs suggesting that the formation activation energy is between ~32 and 56 kJ/mol, in the range for CO oxidation by supported catalysts. Infrared spectroscopy reveals only features due to molecularly adsorbed carbon monoxide suggesting that the CO_2 forms directly without the intervention of any other intermediate species such as carbonates.

Acknowledgements

We gratefully acknowledge the support of this work by the National Science Foundation, under grant number CHE-1,109,377.

References

[1] R.J. Koestner, M.A. Van Hove, G.A. Somorjai, J. Phys. Chem. 87 (1983) 203.
[2] G.A. Somorjai, Langmuir 7 (1991) 3176.
[3] G.A. Somorjai, Catal. Lett. 12 (1992) 17.
[4] G.A. Somorjai, J. Mol. Struct. THEOCHEM 424 (1998) 101.
[5] G.A. Somorjai, J. Phys. Chem. B 104 (2000) 2969.
[6] G.A. Somorjai, J. Phys. Chem. B 106 (2002) 9201.
[7] J. Gong, Chem. Rev. 112 (2012) 2987.
[8] P. Maksymovych, J.T. Yates, J. Am. Chem. Soc. 130 (2008) 7518.
[9] J. Boscoboinik, J. Kestell, M. Garvey, M. Weinert, W. Tysoe, Top. Catal. 54 (2011) 20.
[10] J.A. Boscoboinik, F.C. Calaza, Z. Habeeb, D.W. Bennett, D.J. Stacchiola, M.A. Purino, W.T. Tysoe, Phys. Chem. Chem. Phys. 12 (2010) 11624.
[11] M. Haruta, N. Yamada, T. Kobayashi, S. Iijima, J. Catal. 115 (1989) 301.
[12] M. Haruta, Catal. Today 36 (1997) 153.
[13] G. Hutchings, Gold Bull. 29 (1996) 123.
[14] J. Edwards, P. Landon, A.F. Carley, A.A. Herzing, M. Watanabe, C.J. Kiely, G.J. Hutchings, J. Mater. Res. 22 (2007) 831.
[15] A.A. Herzing, C.J. Kiely, A.F. Carley, P. Landon, G.J. Hutchings, Science 321 (2008) 1331.
[16] A.M. Venezia, L.F. Liotta, G. Pantaleo, V. La Parola, G. Deganello, A. Beck, Z. Koppány, K. Frey, D. Horváth, L. Guczi, Appl. Catal. A Gen. 251 (2003) 359.
[17] L. Guczi, G. Petö, A. Beck, K. Frey, O. Geszti, G. Molnár, C. Daróczi, J. Am. Chem. Soc. 125 (2003) 4332.
[18] C. Xu, J. Su, X. Xu, P. Liu, H. Zhao, F. Tian, Y. Ding, J. Am. Chem. Soc. 129 (2007) 42.
[19] J.-D. Grunwaldt, C. Kiener, C. Wögerbauer, A. Baiker, J. Catal. 181 (1999) 223.
[20] Y. Liu, C.-J. Jia, J. Yamasaki, O. Terasaki, F. Schüth, Angew. Chem. Int. Ed. 49 (2010) 5771.
[21] M. Comotti, W.-C. Li, B. Spliethoff, F. Schüth, J. Am. Chem. Soc. 128 (2006) 917.
[22] M. Valden, S. Pak, X. Lai, D.W. Goodman, Catal. Lett. 56 (1998) 7.
[23] M. Haruta, J. New Mater. Electrochem. Syst. 7 (2004) 163.
[24] T. Fujitani, I. Nakamura, M. Haruta, Catal. Lett. 144 (2014) 1475.
[25] J. Saavedra, H.A. Doan, C.J. Pursell, L.C. Grabow, B.D. Chandler, Science 345 (2014) 1599.
[26] M. Date, M. Haruta, J. Catal. 201 (2001) 221.
[27] M. Date, M. Okumura, S. Tsubota, M. Haruta, Angew. Chem. Int. Edit. 43 (2004) 2129.
[28] R.A. Ojifinni, N.S. Froemming, J. Gong, M. Pan, T.S. Kim, J.M. White, G. Henkelman, C.B. Mullins, J. Am. Chem. Soc. 130 (2008) 6801.
[29] T.S. Kim, J. Gong, R.A. Ojifinni, J.M. White, C.B. Mullins, J. Am. Chem. Soc. 128 (2006) 6282.
[30] J. Michael Gottfried, K. Christmann, Surf. Sci., 566–568, Part 2 (2004) 1112.
[31] B.K. Min, A.R. Alemozafar, D. Pinnaduwage, X. Deng, C.M. Friend, J. Phys. Chem. B 110 (2006) 19833.
[32] X.Y. Deng, B.K. Min, A. Guloy, C.M. Friend, J. Am. Chem. Soc. 127 (2005) 9267.
[33] V.A. Bondzie, S.C. Parker, C.T. Campbell, J. Vac. Sci. Technol. A 17 (1999) 1717.
[34] M.M. Schubert, S. Hackenberg, A.C. van Veen, M. Muhler, V. Plzak, R.J. Behm, J. Catal. 197 (2001) 113.
[35] J.D. Grunwaldt, A. Baiker, J. Phys. Chem. B 103 (1999) 1002.
[36] H. Hakkinen, U. Landman, J. Am. Chem. Soc. 123 (2001) 9704.
[37] P. Konova, A. Naydenov, C. Venkov, D. Mehandjiev, D. Andreeva, T. Tabakova, J. Mol. Catal. A Chem. 213 (2004) 235.
[38] R.A. Ojifinni, J. Gong, N.S. Froemming, D.W. Flaherty, M. Pan, G. Henkelman, C.B. Mullins, J. Am. Chem. Soc. 130 (2008) 11250.
[39] J. Kim, E. Samano, B.E. Koel, J. Phys. Chem. B 110 (2006) 17512.
[40] M.L. Kottke, R.G. Greenler, H.G. Tompkins, Surf. Sci. 32 (1972) 231.
[41] L. Piccolo, D. Loffreda, F. Aires, C. Deranlot, Y. Jugnet, P. Sautet, J.C. Bertolini, Surf. Sci. 566 (2004) 995.
[42] C. Ruggiero, P. Hollins, J. Chem. Soc. Faraday Trans. 92 (1996) 4829.
[43] N. Saliba, D.H. Parker, B.E. Koel, Surf. Sci. 410 (1998) 270.
[44] P.A. Redhead, Vacuum 12 (1962) 9.
[45] K. Nakamoto, Infrared and Raman Spectra of Inorganic and Coordination Compounds, Wiley, New York, 1997.
[46] M. Mihaylov, H. Knozinger, K. Hadjiivanov, B.C. Gates, Chem. Ing. Tech. 79 (2007) 795.
[47] M. Kaltchev, A.W. Thompson, W.T. Tysoe, Surf. Sci. 391 (1997) 145.
[48] S.D. Senanayake, D. Stacchiola, P. Liu, C.B. Mullins, J. Hrbek, J.A. Rodriguez, J. Phys. Chem. C 113 (2009) 19536.
[49] P. Dumas, R.G. Tobin, P.L. Richards, Surf. Sci. 171 (1986) 555.
[50] P. Dumas, R.G. Tobin, P.L. Richards, J. Electron Spectrosc. Relat. Phenom. 39 (1986) 183.
[51] Y. Jugnet, F. Aires, C. Deranlot, L. Piccolo, J.C. Bertolini, Surf. Sci. 521 (2002) L639.
[52] K.F. Peters, P. Steadman, H. Isern, J. Alvarez, S. Ferrer, Surf. Sci. 467 (2000) 10.
[53] B. Hammer, Y. Morikawa, J.K. Nørskov, Phys. Rev. Lett. 76 (1996) 2141.
[54] G. Blyholder, J. Phys. Chem. 68 (1964) 2772.
[55] T.V.W. Janssens, B.S. Clausen, B. Hvolbaek, H. Falsig, C.H. Christensen, T. Bligaard, J.K. Norskov, Top. Catal. 44 (2007) 15.
[56] C. Lemire, R. Meyer, S. Shaikhutdinov, H.-J. Freund, Angew. Chem. Int. Ed. 43 (2004) 118.
[57] J. Biener, M.M. Biener, T. Nowitzki, A.V. Hamza, C.M. Friend, V. Zielasek, M. Bäumer, ChemPhysChem 7 (2006) 1906.
[58] R.G. Greenler, J. Chem. Phys. 44 (1966) 310.
[59] R.A. Ojifinni, J. Gong, N.S. Froemming, D.W. Flaherty, M. Pan, G. Henkelman, C.B. Mullins, J. Am. Chem. Soc. 130 (2008) 11250.
[60] M.J.P. Hopstaken, J.W. Niemantsverdriet, J. Chem. Phys. 113 (2000) 5457.
[61] J. Küppers, A. Plagge, The Langmuir–Hinshelwood Reaction between Oxygen and CO at Ir(111) Surfaces, Zeitschrift für Naturforschung A1979 81.
[62] T. Matsushima, H. Asada, J. Chem. Phys. 85 (1986) 1658.
[63] J.L. Gland, E.B. Kollin, J. Chem. Phys. 78 (1983) 963.